PCCP

Accepted Manuscript

ROYAL SOCIETY OF CHEMISTRY

www.rsc.org/pccp

A Sum-Frequency Generation Spectroscopic Study of the Gibbs Analysis Paradox: Monolayer or Sub-Monolayer Adsorption?

Afshin Asadzadeh Shahir, Khoi Tan Nguyen, Anh V. Nguyen[*]

School of Chemical Engineering, The University of Queensland, Brisbane, QLD 4072, Australia

[*]Corresponding Authors. Email: anh.nguyen@eng.uq.edu.au; Phone: +61733653665

Abstract

The Gibbs adsorption isotherm (GAI) has been considered as the foundation of surfactant adsorption studies for over a century; however, its application in determining the limiting surface excess has recently been intensively discussed, with contradictory experimental evidence either supporting or refuting the theory. The available arguments are based on monolayer adsorption models. In this paper, we experimentally and intellectually proposed and validate the contribution of sub-monolayer adsorption to the GAI paradox. We utilize a powerful intrinsically surface-sensitive technique, vibrational sum-frequency generation spectroscopy (SFG), complemented with conventional tensiometric measurements to address these controversies both quantitatively and qualitatively. Our SFG results revealed that the precipitous decrease in surface tension directly corresponds to surface occupancy by adsorbates. In addition, the Gibbs analysis was successfully applied to the soluble monolayer of a surface-active alcohol to full saturation. However, the full saturation of the topmost monolayer did not necessarily mean that the surface adsorption was completed because the adsorption was observed to continuously occur at the sub-monolayer region soon after the topmost monolayer became saturated. Nonetheless, the Gibbs isotherm failed to account for the excess of alcohol adsorbed at this sub-monolayer region. This new concept of surface excess must therefore be treated thermodynamically.

Keywords: monolayer adsorption, Gibbs isotherm, multilayer adsorption, surface tension

1. Introduction

During the last century, the mathematical modeling of interfacial adsorption has undoubtedly been the most prevalent approach among surface scientists to gather thermodynamic information regarding the adsorption phenomenon. A tremendous wave of interest in the mathematical description of adsorption and quantification of adsorption parameters was generated after the foundation of thermodynamics of interfaces by Josiah Willard Gibbs in the late 1870s,[1] resulting in the development of numerous adsorption models that are still being used by the community.[2-9] Among these models, the Gibbs adsorption isotherm (GAI) is certainly the cornerstone of classical modeling, from which some other models have been derived; a massive amount of surface-excess data have thus far been calculated for various solutions. The popularity of the isotherm originates from its straightforward approach to relate two measurable properties of surface tension, γ, and bulk activity, a_i , to the non-measurable parameter of interest, i.e., the surface excess of species *i*, Γ_i:[10]

$$\Gamma_i = -\frac{1}{nRT}\left(\frac{d\gamma}{d\ln a_i}\right) \quad (1)$$

where R is the gas constant, T is the absolute temperature, and n is the number of species formed by the dissociation of adsorbates.

The fact that these adsorption models are all derived on the basis of some simplifying assumptions, e.g., monolayer or ideal adsorption, brings an uncertainty to the reliability of their outcomes because a particular system may not necessarily satisfy the assumptions of the model. As a consequence, the selection of an incorrect model produces misleading results that do not reflect the real behavior of the system at all. Thus, the choice of a suitable model

requires a pre-evaluation of the system at the microscopic level. Unfortunately, the inability of the classical models to provide molecular-level information regarding the interface is another inherent shortcoming that limits their applicability. Fortunately, the development of experimental surface-specific techniques during recent decades has enabled surface scientists to directly measure adsorption parameters, and thence, to scrutinize the validity and applicability of the classical adsorption models to certain systems. Among these techniques, the most popular ones for air/liquid interfaces are the radiotracer method,[11, 12] neutron reflectivity,[13] ellipsometry,[14] neutral impact collision ion-scattering spectroscopy,[15] and non-linear optical techniques such as second-harmonic generation[16] and sum-frequency generation spectroscopies.[17]

A notable example of how these techniques can help overcome the aforementioned problems is the recent arguments over the Gibbs analysis of surface-tension data. The issue raised by Menger et al. through their two papers questions the validity of area-per-surfactant values calculated on the basis of the GAI.[18, 19] Although some researchers later attempted to refute the ideas of Menger et al. by conceptually reinterpreting their findings as well as the GAI, they still utilized the classical approach without providing further experimental evidence.[20, 21] The first experimental evidence was provided by Menger et al., who used a radiotracer method to support their claim.[22] The neutron reflectivity (NR) method has also used to resolve this issue by measuring surface excess.[13, 23, 24] Although the findings appear to address some issues of the Gibbs paradox, the recent findings by Moroi et al. demonstrate a different interfacial adsorption model for soluble surfactants,[25-28] suggesting the need for further investigation of similar systems. In the case of such an adsorption mechanism, the applicability of the GAI must be re-evaluated because a new concept of surface excess is introduced.

Here, we address the aforementioned issue by using one of the most powerful intrinsically surface-specific techniques available to investigate the adsorption layers, i.e., sum-frequency generation spectroscopy (SFG).[17] We study the adsorption of methyl isobutyl carbinol (MIBC, or 2-methyl-4-pentanol), a non-aggregating surfactant with substantial surface activity but no bulk micellization. It is widely used as an industrial froth-forming reagent. Along with the qualitative determination of the surface monolayer saturation, orientational stability of the adsorbed MIBC molecules also enables characterization of their adsorption in terms of surface excess through a quantitative interpretation of SFG data. To the best of our knowledge, this work represents the first time that SFG has been used to investigate the aforementioned paradox both quantitatively and qualitatively.

1.1. Gibbs analysis of surface-tension data and the related arguments

In the Gibbs analysis of surface-tension data, a typical $\gamma - \log C$ plot is fitted to either a linear or a polynomial equation[29] to extract the surface-tension slope, $d\gamma / d \ln C$, at any single bulk concentration. The acquired slope is then substituted into Eq. (1) to calculate the surface-excess value. After the surface excess has been calculated, the minimum area per adsorbate molecule, A, is simply calculated using the following equation:

$$A = \frac{10^{18}}{\Gamma \times N_A} \tag{2}$$

where N_A is Avogadro's number. A typical surface-tension plot begins with a plateau (region I) through which surface tension decreases only slightly, followed by a sharp decrease of surface tension (region II), before finally leveling off at the critical micellization concentration (CMC). For a linear region II (constant slope), mathematics requires that the surface excess calculated by the GAI must also have a constant value. This result has been interpreted to indicate surface saturation at the beginning of region II.[30, 31] According to the

GAI, the sharp decrease in γ through region II is then inevitably attributed to the increase in bulk surfactant concentration[20] (or activity[10]). However, such purely mathematical interpretation does not appear to be physically sensible. The GAI implies that an increase in the bulk surfactant activity leads to a decrease in the surface tension through adsorption. Consequently, the adsorption of non-ionic surfactants (and, thus, the surface-tension plot) levels off at the CMC because their activity is expected to remain constant above the CMC.[13] Therefore, surfactant molecules in the bulk substantially affecting the surface tension without any physical interaction (adsorption) with the surface beyond the point of monolayer saturation is difficult to conceive.[18, 22]

This paradox was first discussed by Menger et al. through an alternative model that suggests the progressive adsorption under Frumkin kinetics along the controversial region of linearity.[18] They argued that the assumption of a saturated surface throughout region II and the consequent linear fitting will result in "greatly overestimated" values for area-per-surfactant at saturation. They performed pressure-area measurements for insoluble monolayers of several surfactants to support their hypotheses.[18, 19] Laven and de With later discussed that, although the adsorbed amount hardly changes through region II, it is not perfectly constant.[20] This result implies that a polynomial rather than a linear fitting must be applied to tensiometry plots.[29] They also questioned the practicality of the application of the GAI to monolayers of insoluble surfactants because "the establishment of an equilibrium between the surfactant activities at the surface and in the bulk is doubtful."[20] Shortly afterwards, Bermudez-Salguero and Gracia-Fadrique developed a thermodynamic model to demonstrate that full surface saturation is actually attained at the end of rather than at the beginning of linear region II and immediately before the CMC.[21] They concluded that "the calculation of the molecular areas through the GAI is valid as long as the data employed approach to surface saturation."[21]

To address the aforementioned criticisms, Menger et al. later employed radio isotope measurements pioneered by Nilsson[32] to measure the surface excess directly and independently of the surface tension and bulk solution.[22] They then related the surface coverage to surface-tension data to demonstrate that the saturation along region II varies from 80% at the beginning to 94% at CMC for the studied ionic surfactant; they finally hypothesized that "linearity in region II is not indicative of surface saturation."[22] The investigation of the surface saturation versus the bulk micellization shows that, in the case of non-ionic surfactants, the GAI results are in good agreement with NR measurements.[13] The surface saturation is achieved at or immediately below the CMC, resulting in the linearity of surface-tension plot near the CMC; this linearity allows for successful determination of the limiting slope, and thence, of the limiting surface excess through the GAI. However, a considerable discrepancy exists between the NR measurement results and the GAI predictions in the case of ionic surfactants. Here, surface saturation is preceded by a micellization width, i.e., the slope of region II; consequently, the surface-excess value changes continuously up to the CMC. Because the surfactant bulk activity becomes unknown in the presence of micellization, the GAI cannot successfully predict the saturation adsorption values. Finally, divalent ionic contamination, nonionic impurities, and incomplete wetting in ring and plate tensiometry are other potential sources of the discrepancy between the two methods.[23, 24]

All of the aforementioned discussions have been based on the idea that adsorption can only occur at the topmost surface monolayer, which has the limited capacity of full saturation. However, Moroi et al. have suggested an alternative model for soluble surfactants, where a bimolecular layer adsorbs at deeper interface layers. Using a variety of experimental techniques, including Brewster angle microscopy,[33] evaporation rate measurements,[28] pyrene fluorescence spectroscopy,[26] surface tension[34] and surface potential measurements,[25, 27] they

suggested that well-organized aggregates of soluble surfactants are present at deeper interface layers and that these aggregates tend to decrease solution surface tension through re-organization of the interfacial water molecules. By comparing the surface potential measurements to the surface-tension plots, they have also postulated that the primary plateau in surface-tension plots (region I) is attributable to surface monolayer saturation and that the transition from region I to linear region II is related to the formation of the mentioned sub-surface structures. They also speculated that the sharp linear decrease in region II occurs because of the interfacial water re-structuring caused by sub-surface aggregates while the conventional surface excess remains almost constant.[25, 27] This model depicts a new picture of the interfacial adsorption, which requires a new definition of the surface-excess concept and differs markedly from the conventional monolayer adsorption model that has given rise to the Gibbs analysis paradox.

MIBC provides a very suitable model system to address the aforementioned argument because this non-ionic surface-active alcohol forms a stable, well-oriented surface monolayer whose saturation can be straightforwardly studied over a wide range of concentrations and without any disruption by micellization.[35] In addition, because of the good water solubility of MIBC,[36] thermodynamic equilibrium between the bulk and the adsorbed layers can be established. The experimental evidence provided by our SFG results agrees with a number of previous reports related to sub-surface adsorption models, validates the applicability of the GAI in the analyses of monolayer adsorption and invalidates the applicability of the GAI for analyzing sub-surface adsorption.

1.2 Sum-Frequency Generation Spectroscopy

The theoretical aspects of SFG have been thoroughly reviewed by others.[37-39] However, a brief explanation is provided here to clarify the methodology used for data interpretation.

SFG is a relatively new vibrational spectroscopy technique that is inherently capable of discriminating between interfacial molecules and those in the bulk; i.e., SFG demonstrates excellent surface sensitivity and is therefore one of the most suitable available techniques to study the structure of interfaces and adsorption layers.[17] The SFG technique is based on a second-order non-linear optical phenomenon known as sum-frequency generation; this phenomenon occurs in the presence of intense electrical fields of laser beams. The oscillation of the dipole induced by laser beams in interfacial molecules results in an SFG signal whose frequency is sum of the two incident laser (IR and visible) beams, and its intensity is proportional to the incident intensities, as demonstrated in the following equation:[40]

$$I_{SFG}(\omega_{SFG}) \propto \left| \chi_{eff,NR} + \sum_{q} \frac{A_q}{\omega_{IR} - \omega_q + i\Upsilon_q} \right|^2 I_{IR}(\omega_{IR})\, \mathrm{I}_{vis}(\omega_{vis}) \qquad (3)$$

where A_q is the amplitude of the vibrational mode q; ω_{IR} and ω_q are the frequencies of the input IR and the resonance IR of the vibrational q mode, respectively; and Υ_q describes the damping coefficient of the SFG peak. The first term on the right-hand side of Eq. (3) is the effective non-resonant susceptibility, which varies little with frequency. The second term presents the effective resonant susceptibility, $\chi^{(2)}_{eff,R}$, of the interfacial material. Whenever the input IR frequency coincides with one of the molecular vibrations, an increase in $\chi^{(2)}_{eff,R}$, and consequently, in the SFG signal, is clearly observed. By probing the IR through a range of frequencies, a vibrational spectrum of the interfacial molecules is obtained. This spectrum can be fitted by Eq. (3) to extract spectral features.[40]

$\chi^{(2)}_{eff,R}$ is related to the second-order non-linear susceptibility $\chi^{(2)}$ by the following equation:[40]

$$\chi_{eff}^{(2)} = \left[L(\omega_{SFG}).\hat{e}(\omega_{SFG})\right].\chi^{(2)} : \left[L(\omega_{Vis}).\hat{e}(\omega_{Vis})\right]\left[L(\omega_{IR}).\hat{e}(\omega_{IR})\right] \quad (4)$$

where L is the Fresnel coefficient for the corresponding ω frequency and $\hat{e}$ is the unit polarization vector. The tensor $\chi^{(2)}$ has 27 components that are reduced to the following 4 independent components in the case of an azimuthally isotropic interface:

$$\chi_{xxz}^{(2)} = \chi_{yyz}^{(2)},\ \chi_{xzx}^{(2)} = \chi_{yzy}^{(2)},\ \chi_{zxx}^{(2)} = \chi_{zyy}^{(2)},\ \chi_{zzz}^{(2)} \quad (5)$$

where x, y, and z are the laboratory coordinates. These components can be selectively determined by experimental measurement of $\chi_{eff,R}^{(2)}$ values under four different polarization combinations of ssp, sps, pss, and ppp (where the first, second, and third letters represent the SFG beam, the visible beam, and the IR beam, respectively). The specific form of Eq. (4) for ssp and ppp polarization combinations then becomes:[40]

$$\chi_{ssp}^{(2)} = -L_{yy}(\omega_{SFG})L_{yy}(\omega_{Vis})L_{zz}(\omega_{IR})\sin\alpha_{IR}\chi_{yyz}^{(2)} \quad (6)$$

$$\begin{aligned}\chi_{ppp}^{(2)} = & -L_{xx}(\omega_{SFG})L_{xx}(\omega_{Vis})L_{zz}(\omega_{IR})\cos\alpha_{SFG}\cos\alpha_{Vis}\sin\alpha_{IR}\chi_{xxz}^{(2)} \\ & -L_{xx}(\omega_{SFG})L_{zz}(\omega_{Vis})L_{xx}(\omega_{IR})\cos\alpha_{SFG}\sin\alpha_{Vis}\cos\alpha_{IR}\chi_{xzx}^{(2)} \\ & +L_{zz}(\omega_{SFG})L_{xx}(\omega_{Vis})L_{xx}(\omega_{IR})\sin\alpha_{SFG}\cos\alpha_{Vis}\cos\alpha_{IR}\chi_{zxx}^{(2)} \\ & +L_{zz}(\omega_{SFG})L_{zz}(\omega_{Vis})L_{zz}(\omega_{IR})\sin\alpha_{SFG}\sin\alpha_{Vis}\sin\alpha_{IR}\chi_{zzz}^{(2)}\end{aligned} \quad (7)$$

where α_{SFG} is the reflection angle of the SFG beam, and α_{Vis} and α_{IR} are the incidence angles for the visible and IR beams, respectively.

$\chi_{ijk}^{(2)}$ is, in turn, proportional to both the number density of oscillators that contribute to the signal, N, and the molecular hyper-polarizability averaged over all molecular orientations, $\left\langle \beta_{lmn} \right\rangle$, at the interface:

$$\chi_{ijk}^{(2)} = N\sum_{lmn}\left\langle \mu_{ijk:lmn} \right\rangle \beta_{lmn} \quad (8)$$

β_{lmn} is a tensor whose elements are defined in molecular coordinates (*l*, *m*, *n*); for certain molecular vibrations of certain symmetry, only a few non-zero elements of β exist.[41] $\left\langle \mu_{ijk:lmn} \right\rangle$ is the orientationally averaged Euler angle transformation from the lab coordinates to the molecular coordinates. The specific form of Eq. (8) for the molecules with only one terminal methyl group is available from the literature.[40, 42] However, for MIBC with three methyl groups, the theoretical calculation of β_{lmn} values must be modified (forthcoming publication).

Eq. (8) implies that for a given interface with adsorbed molecules and unchanged geometry of the SFG incoming beams if one conducts two SGF measurements, one measurement under *ssp* polarization combination and the other under *ppp* polarization combination, the ratio $\chi^{(2)}_{zzz,as} / \chi^{(2)}_{yyz,s}$ becomes a function of only molecular tilt angle θ since the number of oscillators (*N*) does not change during the measurements. Experimentally, the value of $\chi^{(2)}_{zzz,as} / \chi^{(2)}_{yyz,s}$ can be determined by calculating the ratio $\chi^{(2)}_{ppp} / \chi^{(2)}_{ssp}$ from the measured values of the SFG signal intensities of the two SFG experiments and applying Fresnel coefficient corrections by Eqs. (6) and (7). If the two SFG measurements are repeated for a series of surfactant concentrations, two scenarios can occur with increasing surfactant concentration: the ratio $\chi^{(2)}_{ppp} / \chi^{(2)}_{ssp}$ increases at first and then remains unchanged. In the first scenario, after having determined the ratio $\chi^{(2)}_{ppp} / \chi^{(2)}_{ssp}$ using the two measured SFG intensities, the molecular orientation distribution at interface can be deduced using the appropriate form of Eq. (8) and the calculated values of β_{lmn}. Therefore, the measured $\chi^{(2)}_{ppp} / \chi^{(2)}_{ssp}$ values can be used to detect the orientational change of MIBC molecules with increasing adsorption at the interface.

In the second scenario, the tilt angle θ does not substantially vary much for two different number densities N and N' at two interfaces of two different surfactant concentrations, then ratio of Eq. (8) obtained for two surfactant concentrations using either the ssp or the ppp polarization combination is independent of orientational changes and is proportional to the number density. Therefore, we must have:

$$\left(\frac{\chi_{N'}^{(2)}}{\chi_{N}^{(2)}}\right)_{yyz} \approx \left(\frac{\chi_{N'}^{(2)}}{\chi_{N}^{(2)}}\right)_{zzz} \approx \frac{N'}{N} \tag{9}$$

By Fresnel coefficient correction for these ratios using Eqs. (6) and (7), the ratio N'/N can then be measured experimentally through measurement of $\left(\chi_{N'}^{(2)}/\chi_{N}^{(2)}\right)_{ssp}$ and/or $\left(\chi_{N'}^{(2)}/\chi_{N}^{(2)}\right)_{ppp}$ ratios from the corresponding SFG spectra. Within experimental errors, the ratio N'/N can then be compared to Γ'/Γ values predicted by adsorption models for the system to evaluate their reliability and applicability.

2. Experimental details

2.1 Materials

MIBC with a purity greater than 99% was purchased from ACROS Organics (Belgium) and used as received. Sodium chloride (purity > 99%) was purchased from Sigma-Aldrich and roasted for 10 h at 600 °C to eliminate any organic contaminants. Purified water (prepared using an Ultrapure Milli-Q unit from Millipore, USA) with a resistivity of 18.2 MΩ·cm was used to prepare all of the solutions in the experiments. For the SFG air-aqueous interface experiments, an MIBC solution of appropriate concentration was introduced into a

thoroughly cleaned reservoir of 20 mL, and then the system was allowed to stand for 10 min to equilibrate.

2.2 Surface-tension measurements

The surface-tension measurements were performed using the Wilhelmy plate method. Any possible organic contaminants on the Pt plate were burnt using a micro-beam flame until the Pt turned bright. Tabulated surface tension of deionized water at the same room temperature was used to calibrate each of the surface-tension measurements. Three successive measurements were taken and averaged for each point. All experiments were performed at room temperature of approximately 23±1 °C.

2.3 Sum-frequency generation spectroscopy

The experimental setup and SFG methodology used in this study have been described elsewhere.[43] Briefly, the visible beam and the tunable IR were overlapped spatially and temporally on the sample. The visible beam was generated by frequency-doubling the fundamental output pulses (1064 nm, 10 Hz) of 20 ps pulse-width from an EKSPLA solid-state Nd:YAG laser. The tunable IR beam was generated from an EKSPLA optical parametric generation/amplification and difference-frequency system based on LBO and $AgGaS_2$ crystals. The temperature and humidity of the laboratory were kept constant to minimize the environmental errors. The geometry of the SFG setup was the same for all measurements.

The SFG spectra were gathered in C-H stretch region from 2800 to 3000 cm^{-1} in both ssp and ppp polarization combinations. The peaks at 2840, 2920, and 2905 cm^{-1} were assigned to the methylene symmetric stretch, asymmetric stretch, and Fermi resonance,

respectively; while the peaks at 2875, 2965, and 2945 cm^{-1} were assigned to the methyl symmetric stretch, asymmetric stretch, and Fermi resonance vibrational modes, respectively (Table 1).[44] The obtained SFG spectra were deconvoluted (Fig. 6) using the Lorentzian line-shape function described by Eq. (3).

3. Results and Discussion

3.1. Monolayer adsorption at surface

The SFG spectra collected for aqueous solutions of MIBC are shown in Fig. 1. Throughout the studied concentration range (5-30 mM), the spectra are obviously dominated by only methyl-group stretches. Without any SF intensity loss, the measured $\chi^{(2)}_{eff,R}$ can be related to the contribution from all interfacial MIBC molecules if the orientational details regarding the adsorbed layer are also available. To achieve this, the spectra must be analyzed quantitatively.

To calculate $\chi^{(2)}_{eff,R}$, the obtained spectra were deconvoluted using Eq. (3) and the A_q and Υ_q values were subsequently extracted. Fig. 2 and Table 1 show the individual peaks and the extracted spectral features for the 30 mM solution of MIBC, respectively. Having determined the values of $\chi^{(2)}_{eff,R}$ for both ssp and ppp polarization combinations, we calculated the $\chi^{(2)}_{ppp}/\chi^{(2)}_{ssp}$ ratio to track the variation of the molecular tilt angle at the interface with the surfactant bulk concentration. Our calculation of MIBC tilt angles revealed that the C-O bond of MIBC adopts an orientation of 39±2° against surface normal (see Fig. S4). With this configuration, the orientation of OH group of MIBC is very similar to that of the hydrogen-bonded OH of the interfacial water molecules. Fig. 3a shows that the $\chi^{(2)}_{ppp}/\chi^{(2)}_{ssp}$ ratio varies

only slightly from 0.83 at 5 mM to 0.78 at 20 mM, where it finally levels off. This very small variation in $\chi^{(2)}_{ppp}/\chi^{(2)}_{ssp}$ corresponds to a maximum fluctuation of about 5° in the tilt angle of MIBC molecules. The hydrogen bonding of the OH group of MIBC with interfacial water molecules apparently has a stabilizing effect that pins the molecules onto the surface and restricts their motion. Nevertheless, the $\chi^{(2)}_{eff,R}$ values, which are proportional to the square root of the SF intensity, detected in both ssp and ppp polarization combinations sharply increase as the bulk MIBC concentration increases from 5 to 12.5 mM. Because the variation in the tilt angle, θ, is very small, this sharp intensity increase is mainly attributed to the continuous adsorption of MIBC molecules, i.e., an increase of *N* in Eq. (8), at the topmost monolayer. Molecular dynamics simulations have already shown that homologous alcohols form a single adsorption layer below surface saturation and that this layer interacts with only a few outermost layers of the interfacial water molecules.[45] When the bulk MIBC concentration exceeds 12.5 mM, although $\chi^{(2)}_{ppp}$ appears to remain mostly constant, $\chi^{(2)}_{ssp}$ continues to slightly increase to its maximum value at 20 mM. Because $\chi^{(2)}_{ppp}/\chi^{(2)}_{ssp}$ also reaches its minimum at this point, we expect a stable and fully saturated monolayer of adsorbed MIBC molecules when the bulk MIBC concentration reaches or exceeds 20 mM.

Such a well-ordered monolayer expectedly applies a net surface potential that originates from the electric dipoles of the adsorbed MIBC molecules. Previous studies have revealed the formation of an electrical double layer that generates a considerable surface potential in MIBC and 1-hexanol solutions.[35, 46] Similar to ionic surfactants, the adsorption of MIBC is therefore expected to increase in the presence of salt. According to Fig. 3b, the addition of 2M NaCl shifts the monolayer saturation point from 20 mM (in the absence of NaCl) to approximately 15 mM, where the ssp intensity and $\chi^{(2)}_{ppp}/\chi^{(2)}_{ssp}$ ratio become almost

constant within the experimental error (see Fig. S1 for the spectra). Such a small shift is attributed to the partial shielding of electrostatic repulsion between the MIBC dipoles by Na^+ and Cl^- ions close to the surface. The range of $\chi^{(2)}_{ppp}/\chi^{(2)}_{ssp}$ variation with MIBC concentration is greater here (> 0.1) compared to variation in the case of the salt-free MIBC solution (≈ 0.05); i.e., the MIBC molecules appear to have more freedom of motion at lower surface packing because the hydrogen bonding between MIBC and interfacial water molecules is disrupted by the salt ions. Nevertheless, the variation in $\chi^{(2)}_{ppp}/\chi^{(2)}_{ssp}$ is sufficiently small for the change in tilt angle to be neglected. Furthermore, the final value of $\chi^{(2)}_{ppp}/\chi^{(2)}_{ssp}$ (0.76) is approximately the same as that for salt-free solution (0.78). This result indicates that compression of the saturated MIBC monolayer by such a high concentration of NaCl has only a negligible effect on the tilt angle of the adsorbed molecules. The dipole-dipole repulsion and the steric effect of alkyl chains do not appear to be sufficiently strong to dominate the stabilizing effect of hydrogen bonding by the OH groups.

Fig. 4a shows the surface-tension plots for MIBC solutions with and without 2M NaCl. Despite the appearance of the plots, determining by eye whether region II is linear or curved is difficult. To overcome this problem, we fitted the plots using both a linear and a third-order polynomial equation.[29] The obtained slopes were then substituted into Eq. (1) to calculate the surface-excess values. The surface excess determined by polynomial fitting will therefore be increasing continuously (Fig. 4b). The SFG measurements have successfully and independently shown where the surface monolayer actually becomes saturated. Hence, the GAI-calculated surface excess values for 20 mM MIBC and 15 mM MIBC/2M NaCl solutions were taken as the surface excess of MIBC at monolayer saturation (Table 2).

Table 2 lists the calculated results. As evident in the table, the prediction of linear fitting satisfactorily agrees with that of the polynomial fitting. Using the linear fitting values,

the surface excess of MIBC at monolayer saturation is therefore taken to be 4.4 and 5.0 μmol/m^2 in the absence and in the presence of 2M NaCl, respectively; i.e., the GAI predicts that the addition of 2M NaCl to an MIBC solution will increase the saturation adsorption of MIBC by only 14%. Compared to ionic surfactants,[10] this small increase in the presence of such a high salt concentration confirms that dipole-dipole repulsions and steric effects are not very strong in the case of MIBC. Nonetheless, the increase of pC_{20} (negative logarithm of the minimum surfactant concentration required to lower γ by 20 mN/m) from 1.75 to 2.15 indicates an increase in adsorption efficiency; i.e., MIBC molecules tend to fill the surface monolayer faster, but the final amount of surface excess is only 14% higher compared to the MIBC/water solution. The observed increase in adsorption efficiency is attributed to the decrease in water solubility of MIBC. The solubility of MIBC at 20 °C is approximately 170 mM;[36] this solubility was observed to decrease to approximately 50 mM in the presence of 2M NaCl and even further decreased to 20 mM in the presence of 4M NaCl so that the MIBC droplets were apparently floating on the solution. As the salt ions are added, the water molecules favorably solvate them, thereby expelling the MIBC molecules to the interfacial region.

As evident in Figs. 3a and 3b, both $\chi^{(2)}_{ssp}$ and $\chi^{(2)}_{ppp}$ have higher values in the presence of 2 M NaCl (the spectra are illustrated in Figs. S2 and S3). As previously discussed, the MIBC tilt angle at saturation is not substantially affected by the presence of NaCl. Thus, this increment originate from the increase in adsorption of MIBC, as predicted by the GAI. Because the increase of surface excess does not cause a considerable change in the local electrical field,[40] the refractive index of surface monolayer and the Fresnel coefficients for the saturated monolayers of MIBC in both solutions should not change. On the basis of the discussion in section 2, we have:

$$\left(\frac{\chi^{(2)}_{NaCl+MIBC}}{\chi^{(2)}_{MIBC}}\right)_{ssp} \approx \left(\frac{\chi^{(2)}_{NaCl+MIBC}}{\chi^{(2)}_{MIBC}}\right)_{ppp} \approx \frac{N'}{N} \approx \left(\frac{\Gamma_{NaCl+MIBC}}{\Gamma_{MIBC}}\right)_{GAI} = 1.14 \quad (10)$$

That is, the ratio of measured susceptibilities must be very similar, within the experimental errors, to the predictions of the GAI through linear fitting. If so, this finding would be a mutual validation of both Gibbs analysis and our experimental SFG method. Fig. 5a illustrates the measured $\chi^{(2)}_{eff,R}$ ratio for different MIBC concentrations in the presence and absence of NaCl. The ratio clearly decreases from 1.28 to approximately 1.13 and 1.09 for ssp and ppp measurements, respectively, and becomes constant at approximately 20 mM, where both surface monolayers are fully saturated. This result indicates that the population of MIBC at a saturated monolayer increases by approximately 9-13% in the presence of 2M NaCl.

Although the value obtained from ppp measurements (9%) differs from the value predicted by the GAI (14%), ssp measurements appear to provide a more reliable result (13%) that is meaningfully similar to the GAI result (The Fresnel coefficient of the ssp polarization combination is greater than that of the ppp polarization combination by a factor of 3. The ssp SFG signals are thus more sensitive and reliable than the ppp SFG signals). This small difference between the GAI and SFG results is acceptable within the following errors: (*i*) the experimental errors during SFG and surface-tension measurements likely represent the largest contributions to this difference; (*ii*) the fitting errors; and (*iii*) the slight variations in molecular tilt angle and Fresnel coefficients that were assumed to be negligible during our calculations. Thus, we believe that the agreement between the GAI results and our experimental SFG results is very good, and the linear fitting of surface-tension data beyond monolayer saturation apparently gives reliable values for the surface excess of MIBC at the topmost surface monolayer. When the Fresnel coefficients are known and the orientation distribution of adsorbed MIBC molecules has been calculated, the absolute number of MIBC

molecules at monolayers can also be calculated. Notably, however, the contribution of the aforementioned errors may result in values that differ substantially from the Γ values predicted by the GAI, and thus, will not be useful in interpreting the validity of Gibbs analysis. However, in the case of $\chi^{(2)}$ ratios, the contribution of errors to the denominator and numerator will cancel each other to a great extent, resulting in more consistent values in the case of the GAI predictions.

Aggregating non-ionic surfactants are known to form micelles soon after surface saturation. This formation of micelles is observed in the surface-tension plots as a CMC point at which the plot levels off because the bulk activity is almost constant in the presence of micelles and because the addition of surfactant molecules to the surface stops. As a result, the surface-tension plot becomes linear immediately below the CMC, thereby enabling the GAI to be used successfully. The surface-excess values collected for non-ionic surfactants using this method have been demonstrated to be highly consistent with the results of direct NR measurements.[13] In the case of MIBC, with no CMC, the surface tension still continues to decrease sharply even after full monolayer saturation. Fig. 4a demonstrates that the slope does not change around monolayer saturation. Thus, the linear fitting applied to the lower region of the surface-tension plot (beyond monolayer saturation) gives reliable predictions by the GAI, as previously confirmed through our measured $\chi^{(2)}_{eff,R}$ ratios (Fig. 5a). Our SFG results, along with others' experimental findings,[13, 22-24, 47] demonstrate that adsorption proceeds progressively throughout region II. Thus, the surface should not already be saturated in the beginning of region II, as had been previously hypothesized. We conjecture that the Gibbs analysis paradox originated from the assumption that region II is perfectly linear from its beginning to the CMC; however, we have demonstrated here that the visual evaluation of the linearity of the surface-tension plot can lead to such misinterpretations. Although both linear and polynomial equations fitted our surface-tension data very well (R^2 = 0.999),

judging whether region II is linear or curved is difficult. In this regard, surface-specific techniques such as SFG can effectively provide a direct approach to tracking surface saturation.

3.2. Sub-monolayer adsorption

One may wonder how MIBC molecules behave in the bulk after monolayer saturation, knowing that they lack micellization. The elucidation of such behavior will also reveal the origin of the continuing surface tension decrease after monolayer saturation. As previously mentioned, the GAI mathematically implies that, for a constant value of Γ, any further decrease in surface tension must originate from an increase in the bulk activity[10] or concentration.[20] This justification, however, implies a non-physical effect. We also investigated the adsorption behavior of solutions with constant MIBC concentrations of 10 and 20 mM in the presence of 2.5, 5, 1, 2, and 3 M NaCl. We demonstrated that the surface in the absence of salt is partially saturated for 10 mM MIBC solution, but fully saturated for 20 mM MIBC solutions. Therefore, the variation in $\chi^{(2)}_{eff,R}$ and in the $\chi^{(2)}_{ppp}/\chi^{(2)}_{ssp}$ ratio is expected to be small for these solutions (Figs. 3c and 3d). As the concentration of NaCl reaches approximately 1M, the variation in the measured $\chi^{(2)}_{eff,R}$ values begins to decrease, indicating that surface monolayer is almost saturated. In the case of 20 mM MIBC solution, the surface monolayer actually switches from being saturated in the absence of NaCl to being saturated in the presence of NaCl as the salt concentration is increased from 0 to 3 M. On the basis of the previous discussion, we expect that the final variation in the value of $\chi^{(2)}_{eff,R}$ must approach the GAI prediction of a 14% Γ increase in salt solution (Eq. (10)). The data labels in Fig. 3d represent the $\chi^{(2)}_{eff,R}$ increase percentages. Again, our SFG measurements confirm that surface excess at monolayer saturation increases by 10-14% in the presence of NaCl, demonstrating excellent agreement with the GAI's prediction.

Fig. 6 illustrates the results of the surface-tension measurements for 10 mM, 15 mM, and 20 mM MIBC solutions containing NaCl at various concentrations. The surface tension begins to decrease sharply only after the addition of 1M NaCl, where the surface monolayer was already observed to be almost saturated. Because the addition of NaCl noticeably reduces the water solubility of MIBC, the bulk concentration of MIBC decreases. According to the GAI, the surface tension must consequently increase; however, it actually does not. Instead, a substantial decrease as large as 10 mN/m in the surface tension is observed upon the addition of 4M NaCl to 20 mM MIBC solution. In addition, the final $\chi^{(2)}$ values for both 10 mM and 20 mM MIBC solutions ($\chi_{10}^{(2)}$ and $\chi_{20}^{(2)}$) are expected to be the same at monolayer saturation. Fig. 5b clearly confirms this expectation, as $\chi_{20}^{(2)}/\chi_{10}^{(2)}$ becomes constant at approximately 1.02. If the monolayer adsorption were the only process to affect solution surface tension, then the surface tension for both of these solutions would have the same value after monolayer saturation. However, a noticeable difference of 5-6 mN/m between the surface tension of two solutions suggests otherwise (Fig. 6). We mathematically attribute this difference to the difference in bulk MIBC concentrations through the GAI again. In this case, the surface tension of 15 mM MIBC solution must also have been different from that of both solutions. However, the surface tensions of the 15 mM and 20 mM MIBC solutions interestingly begin to converge immediately after the addition of 1M NaCl (Fig. 6).

All these experimental observations clearly demonstrate that the sharp surface tension decrease in Fig. 6 is caused neither through monolayer adsorption nor by the increase in bulk MIBC concentration, as is mathematically inferred from the GAI. We here hypothesize an alternative model that successfully explains the aforementioned observations through the ongoing adsorption of MIBC molecules at the sub-monolayer region after complete saturation of the topmost surface monolayer. The blindness of SFG to deeper layers of a

surface region precludes the direct investigation of sub-monolayer adsorption. The competition between MIBC molecules and salt ions for being solvated by water molecules in the bulk forces them to migrate toward the interfacial region. In addition, unlike its longer-chain homologues such as 1-dodecanol, which are capable of aggregating in the bulk, the relatively shorter chain length of MIBC together with its multiple OH groups makes it difficult for the molecules to form stable aggregates in the bulk to avoid unfavourable water/tail interactions. Aggregation in this case may require the deformation of OH solvation shell or disturbance of its hydrogen-bonding network because of its inner location on the hydrocarbon chain. Hence, even if the surface monolayer is already saturated, the sub-monolayer region will still be accessible for MIBC molecules as an additional adsorption site. This sub-monolayer adsorption apparently represents the main contribution to the decrease in surface tension observed in Fig. 6. After surface monolayer saturation, the number of bulk MIBCs replaceable by salt ions continues to decrease with increasing concentration of NaCl. Because the molar fraction of MIBC is smaller in the 10 mM MIBC solution, the number of MIBC molecules replaced in bulk and then adsorbed at the sub-monolayer region will also be lower in comparison to the two other solutions. As a result, the sub-monolayer excess is expected to be lower for the first solution than for the other two solutions. However, in the case of 15 mM and 20 mM MIBC solutions, a substantial number of MIBC molecules remain in the bulk even after monolayer saturation. In the presence of the same NaCl concentration, the number of replaced MIBCs, the sub-monolayer excess as well as the resulting decrease in surface tension will consequently be approximately the same for the 15 mM and 20 mM MIBC solutions but substantially different from those for the 10 mM MIBC solution. These results clearly demonstrate the availability of the sub-monolayer region for further MIBC adsorption after full saturation of the topmost monolayer. Similarly, in the proposed model,

the precipitous linear decrease of surface tension after monolayer saturation in Figs. 3a and 3b is attributable to the ongoing sub-monolayer adsorption.

Consistent with our findings, other researchers have reported similar observations regarding the structuring of soluble surfactants at deeper layers of water surfaces. Neutron specular reflection studies of tetradecyltrimethylammonium bromide (TTAB) solution have revealed the adsorption of a layer of aggregated micelles at concentrations far greater than the CMC, with its center located approximately 90 Å from the center of the surface monolayer. A depletion layer containing only water molecules has also been proposed to exist between two surfactant layers.[48] The ordering of this water layer is likely another source of the changes in solution surface tension and surfactant adsorption.[26] Interestingly, this model has also been confirmed by computer simulations.[49] Another model suggests that the structure of the adsorbed layer of soluble surfactants differs from that of conventional surface monolayers of insoluble surfactants. Whereas the latter is located on the outermost layer of the air/water surface, the former is in the form of a bimolecular layer located "at a certain distance below the surface."[26-28, 33, 34] However, this model was later modified through surface potential measurements to consider a soluble monolayer adsorbed at the topmost surface layer along with an adsorbed bilayer some distance beneath the monolayer with a depletion layer of ordered water molecules located between two surfactant layers. The linearity of surface-tension plots has also been related to the formation of this immersed surfactant bilayer, during which the surface excess of the topmost monolayer remains constant but the re-arrangement of the confined interfacial water molecules reduces solution surface tension.[25] This model is very similar to that suggested by Lu et al.[48] Further evidence for such a multilayer adsorption at an air/water interface is also discussed in the literature.[50]

Despite the aforementioned models generally being in excellent agreement with our current findings, some substantial differences exist in the details. First, the strong SF spectra

from MIBC solutions clearly indicate the presence of an adsorbed monolayer, unlike the preliminary models by Moroi et al.[28, 33] Second, the inability of MIBC molecules to form micelles eliminates the possibility for aggregation of micelles at deeper layers of the surface, as previously proposed.[48, 49] Finally, the formation of a bilayer immersed at a depth within the operating range of SFG instead of a surface monolayer could not be expected for MIBC because the SFG signals from a bilayer would be cancelled out. Molecular dynamics simulations for some alcohols' homologues with MIBC, e.g., pentanol, octanol, and dodecanol, have revealed that these molecules mainly interact with only the topmost water layer of interface at lower packing. However, a second layer of alcohol molecules appears immediately below the topmost adsorbed monolayer as the surface density increases from 1 to 4 μmol/m^2.[45] On this basis, our rough model proposes that MIBC molecules fill subsequent adsorption layers immediately below the saturated topmost monolayer, whose excess is not accounted for by the GAI through linear fitting to surface-tension data. However, the true structure of this sub-monolayer adsorption layer remains an open question. The proposed model is schematically illustrated in Fig. 7.

4. Conclusion

For the first time, we applied SFG to study the adsorption of a special surface-active alcohol, MIBC, to respond to the recent controversy over the applicability of the GAI to analysis of surface-tension data. This paradox is critical to surface science because the GAI has been serving as the thermodynamic foundation of adsorption calculations for more than a century. Qualitatively, SFG was used to monitor the formation of a fully saturated surface monolayer directly, independent of the bulk. Within the experimental errors, our quantitative approach also successfully demonstrated that the linear fitting to the post-saturation part of the surface-tension plot gives reliable values for surface excess of the adsorbed monolayer at saturation, implying that the plot actually becomes linear only after full monolayer saturation.

These results are important because visually determining where the plot becomes linear (or where surface becomes saturated) is difficult. The surface-tension plot is conventionally supposed to level off at CMC in the case of aggregating non-ionic surfactant solutions. Nonetheless, for non-aggregating MIBC molecules, a sub-monolayer region was observed to provide another adsorption site. Although the GAI can successfully predict the surface excess of the topmost monolayer through linear fitting, it clearly fails to account for the additional surface excess adsorbed in the sub-monolayer region. This sub-monolayer adsorption was observed to substantially contribute to the solution surface tension; i.e., the actual surface excess of MIBC is higher than what is calculated by the GAI for the saturated monolayer. As a consequence, a new concept of surface excess emerges, as also suggested by others.[48] Because the sub-monolayer region did not contribute to the SF signal, neither its structure nor its composition could be investigated by SFG. However, we proposed that a second layer of MIBC adsorbed immediately below the topmost monolayer. This model was hypothesized by matching our SFG results to surface-tension data and is supported by computer simulations for similar alcohol solutions.[45] Neutron reflectivity can also be used as a suitable complementary technique to determine the surface excess of this sub-monolayer adsorption, although careful calibration is required to avoid elimination of its contributing signal as a background signal.[48] In summary, although the linearity of the lower part of surface-tension plot was observed to be correlated with full saturation of the surface topmost monolayer, it never represented the end of adsorption at the interfacial region. Instead, our alternative sub-monolayer adsorption model suggests that adsorption of MIBC at a deeper part of the surface is ongoing. We here demonstrated that monolayer saturation, at least for MIBC, does not necessarily mean a completed surface saturation.

Because the interpretation of adsorption mechanisms through classical models can provoke serious controversies such as the Gibbs analysis paradox, we applied a surface-

specific technique, SFG, to provide a reliable approach for the direct investigation of adsorption, both qualitatively and quantitatively. We also demonstrated the importance of direct pre-evaluation of a certain surfactant system prior to choosing an adsorption model to extract thermodynamic data and before generalizing the findings for a certain surfactant systems to the adsorption of all similar surfactants. On this basis, we are careful in extrapolating our findings for MIBC to other soluble surfactant solutions; i.e., we believe that a certain surfactant system may have specific physicochemical characteristics and adsorption behavior of its own that can only be understood through direct surface-sensitive methods rather than by intrinsically generalized classical models, just as we demonstrated here for MIBC adsorption.

Acknowledgments

This research has been supported under Australian Research Council's Projects funding schemes (project numbers LE0989675). The University of Queensland is acknowledged for the IPRS postgraduate scholarships provided to the first author (AAS).

References

1. H. A. Bumstead, R. G. Van Name and W. R. Longley, *The Collected Works of J. Willard Gibbs*, Longmans, Green and Co., 1928.
2. E. H. Lucassen-Reynders, *Journal of Physical Chemistry*, 1966, **70**, 1777-1785.
3. J. F. Baret, *J. Colloid Interf. Sci.*, 1969, **30**, 1-12.
4. J. H. de Boer, *The Dynamical Character of Adsorption*, Clarendon Press, Oxford, 1953.
5. E. Helfand, H. L. Frisch and J. L. Lebowitz, *Journal of Chemical Physics*, 1961, **34**, 1037-1042.
6. B. Szyszkowski, *Z Phys. Chem.* , 1908, **64**, 385
7. I. Langmuir, *Journal of the American Chemical Society*, 1918, **40**, 1361-1403.
8. A. N. Frumkin, *Z Phys. Chem.* , 1925, **116**, 466.
9. M. Volmer, *Z Phys. Chem.* , 1925, **115**, 253.

10. M. J. Rosen, *Surfactants and Interfacial Phenomena*, Wiley, Chichester, U.K., 3rd edn., 2004.

11. J. K. Dixon, A. J. Weith Jun, A. A. Argyle and D. J. Salley, *Nature*, 1949, **163**, 845-845.

12. G. Aniansson and O. Lamm, *Nature* 1950, **165**, 357-358.

13. P. X. Li, Z. X. Li, H.-H. Shen, R. K. Thomas, J. Penfold and J. R. Lu, *Langmuir*, 2013, **29**, 9324-9334.

14. R. M. A. Azzam and N. M. Bashara, *Ellipsometry and Polarized Light* North-Holland Publication, Amsterdam, 1979.

15. G. Andersson and H. Morgner, *Surface Science*, 1998, **405**, 138-151.

16. R. M. Corn and D. A. Higgins, *Chem. Rev.*, 1994, **94**, 107-125.

17. G. L. Richmond, *Chem. Rev.* , 2002, ***102***, 2693–2724.

18. F. M. Menger, L. Shi and S. A. A. Rizvi, *J. Am. Chem. Soc.*, 2009, **131**, 10380-10381.

19. F. M. Menger, L. Shi and S. A. A. Rizvi, *Langmuir*, 2010, **26**, 1588-1589.

20. J. Laven and G. de With, *Langmuir*, 2011, **27**, 7958-7962.

21. C. Bermúdez-Salguero and J. Gracia-Fadrique, *J. Colloid Interf. Sci.*, 2011, **355**, 518-519.

22. F. M. Menger, S. A. A. Rizvi and L. Shi, *Langmuir*, 2011, **27**, 7963-7965.

23. P. X. Li, R. K. Thomas and J. Penfold, *Langmuir*, 2014, **30**, 6739-6747.

24. H. Xu, P. X. Li, K. Ma, R. K. Thomas, J. Penfold and J. R. Lu, *Langmuir*, 2013, **29**, 9335-9351.

25. H. Nakahara, O. Shibata, M. Rusdi and Y. Moroi, *Journal of Physical Chemistry C*, 2008, **112**, 6398-6403.

26. R. Humphry-Baker, M. Grätzel and Y. Moroi, *Langmuir*, 2006, **22**, 11205-11207.

27. H. Nakahara, O. Shibata and Y. Moroi, *Langmuir*, 2005, **21**, 9020-9022.

28. M. Rusdi, Y. Moroi, H. Nakahara and O. Shibata, *Langmuir*, 2005, **21**, 7308-7310.

29. I. Mukherjee, S. P. Moulik and A. K. Rakshit, *J. Colloid. Interf. Sci.*, 2013, **394**, 329-336.

30. F. van Voorst Vader, *Trans. Faraday. Soc.*, 1960, **56**, 1067-1077.

31. F. M. Menger, A. L. Galloway and M. E. Chlebowski, *Langmuir*, 2005, **21**, 9010-9012.

32. G. Nilsson, *Journal of Physical Chemistry*, 1957, **61**, 1135-1142.

33. Y. Moroi, M. Rusdi and I. Kubo, *J. Phys. Chem. B*, 2004, **108**, 6351-6358.

34. M. Rusdi, Y. Moroi, T. Hlaing and K. Matsuoka, *B Chem. Soc. Jpn.*, 2005, **78**, 604-610.

35. C. M. Phan, H. Nakahara, O. Shibata, Y. Moroi, T. N. Le and H. M. Ang, *Journal of Physical Chemistry B*, 2012, **116**, 980-986.

36. R. D. Crozier and R. R. Klimpel, *Mineral Processing and Extractive Metallurgy Review*, 1989, **5**, 257-279.

37. A. G. Lambert and P. B. Davies, *Appl. Spectrosc. Rev.*, 2005, **40**, 103-145.

38. M. R. Watry, PhD Thesis, University of Oregon, 2002.

39. W. Hua, PhD Thesis, The Ohio State University, 2013.

40. X. Zhuang, P. B. Miranda, D. Kim and Y. R. Shen, *Phys. Rev. B*, 1999, **59**, 12632-12640.

41. C. Hirose, N. Akamatsu and K. Domen, *Journal of Chemical Physics*, 1992, **96**, 997-1004.

42. J. Wang, C. Chen, S. M. Buck and Z. Chen, *Journal of Physical Chemistry B*, 2001, **105**, 12118-12125.

43. K. T. Nguyen and A. V. Nguyen, *Soft Matter*, 2014, **10**, 6556-6563.

44. J. Liu and J. C. Conboy, *Langmuir*, 2005, **21**, 9091-9097.

45. N. Abrankó-Rideg, M. Darvas, G. Horvai and P. Jedlovszky, *Journal of Physical Chemistry B*, 2013, **117**, 8733-8746.

46. C. V. Nguyen, C. M. Phan, H. M. Ang, H. Nakahara, O. Shibata and V. Moroi, *Journal of Physical Chemistry B*, 2013, **117**, 7615-7620.

47. S. W. An, J. R. Lu, R. K. Thomas and J. Penfold, *Langmuir*, 1996, **12**, 2446-2453.

48. J. R. Lu, E. A. Simister, R. K. Thomas and J. Penfold, *J. Phys. Chem.* , 1993, **97**, 13907-13913.

49. B. Smit, P. A. J. Hilbers, K. Esselink, L. A. M. Rupert, N. M. Van Os and A. G. Schlijper, *Journal of Chemical Physics*, 1991, **95**, 6361-6368.

50. R. K. Thomas and J. Penfold, *Langmuir*, 2015, **31**, 7440-7456.

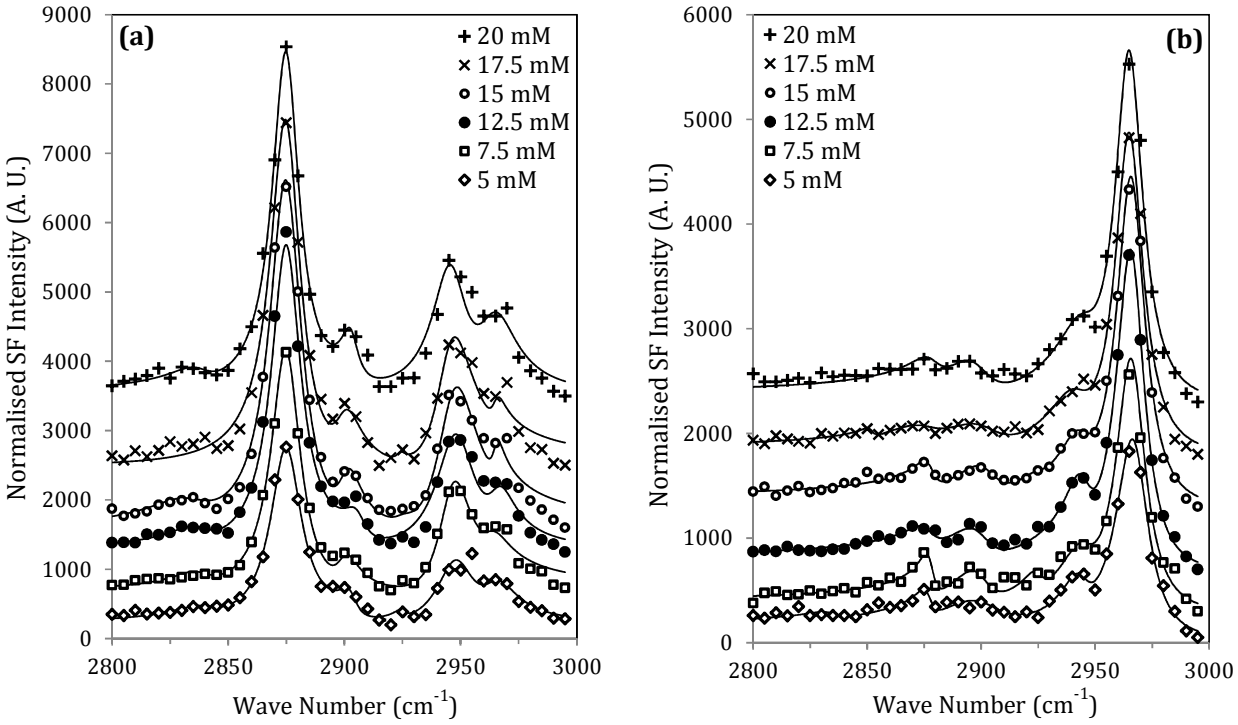

Figure 1. IR- and visible-normalised SF spectra recorded for various concentrations of MIBC in water under (a) ssp and (b) ppp polarization combinations. The solid lines represent the best fittings to the spectra. Note that the spectra are offset by different values for clarity.

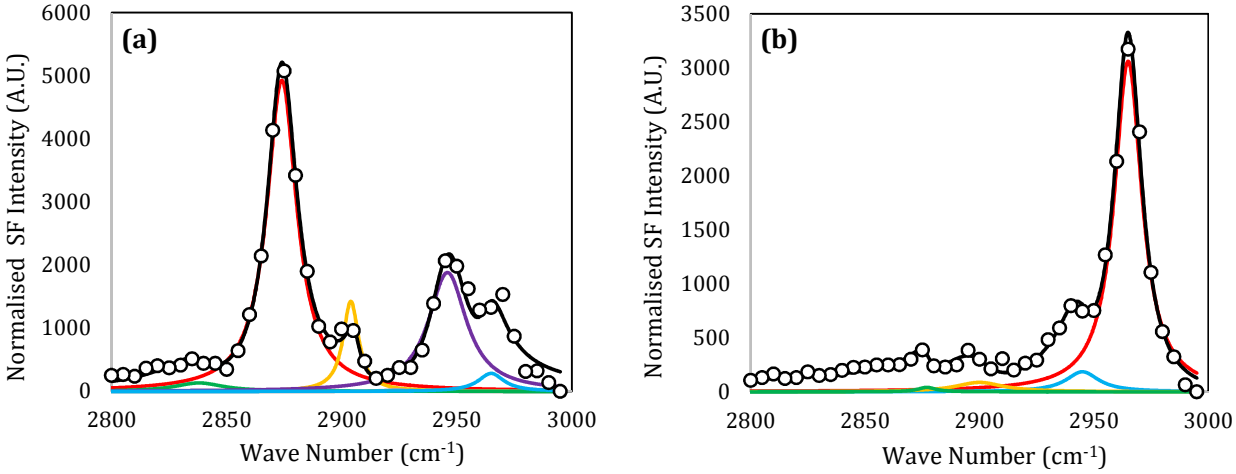

Figure 2. De-convolution of the SF spectrum for 30 mM MIBC solution under (a) ssp and (b) ppp polarisation combinations. The black lines represent the overall best fittings to the spectra.

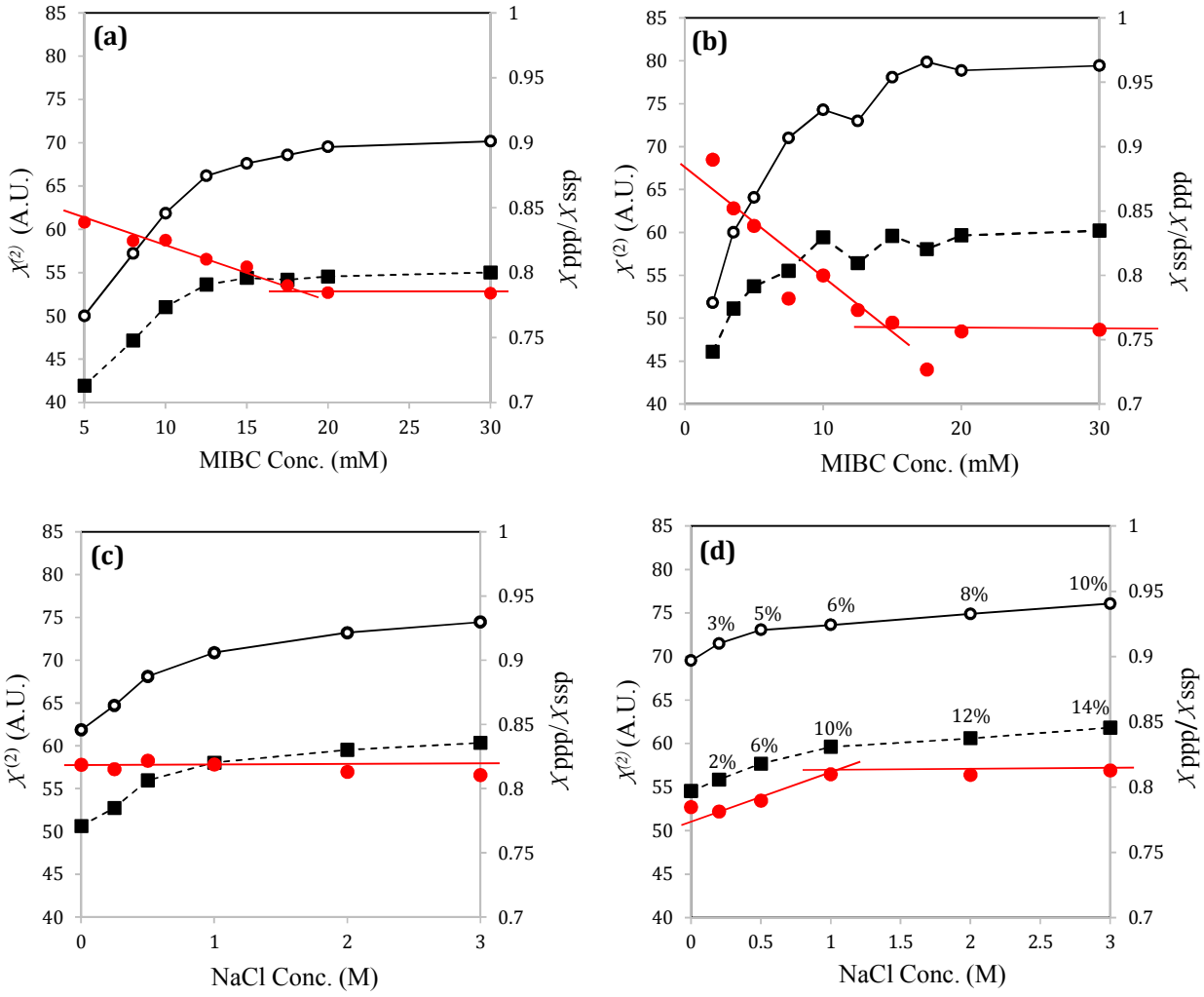

Figure 3. Variation of the effective susceptibility under ssp (○) and ppp (■) polarization combinations and their ratio (●) with the concentration of (a) MIBC in water, (b) MIBC in 2M NaCl, (c) NaCl in 10 mM MIBC, and (d) NaCl in 20 mM MIBC.

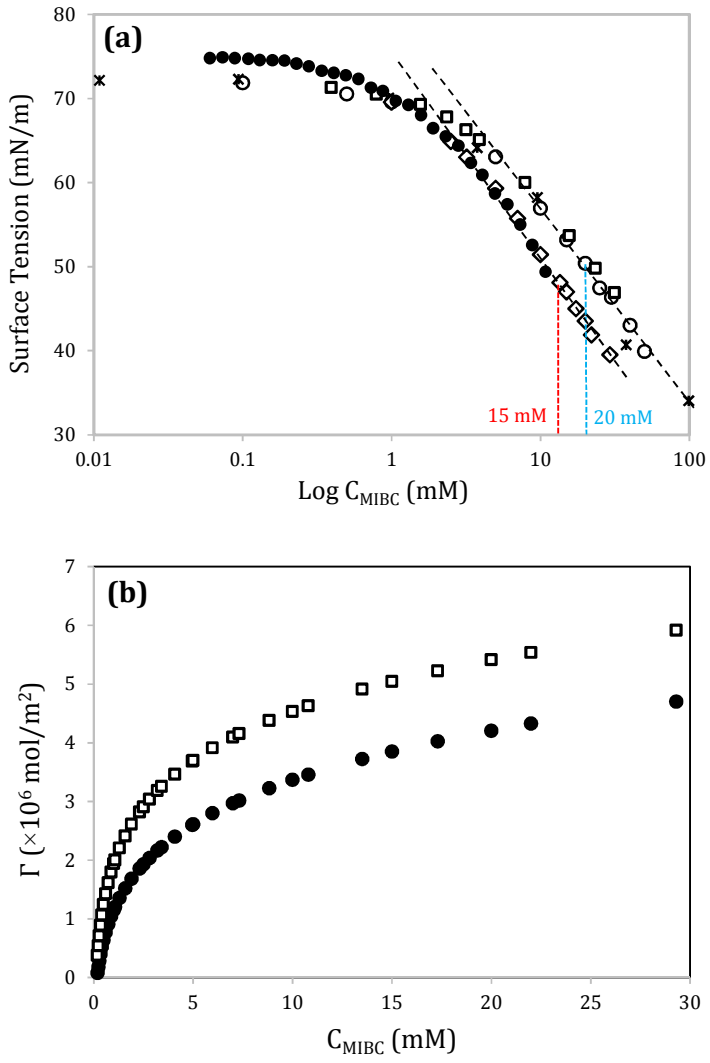

Figure 4. Panel (a): surface tension data measured for MIBC solutions by us (○), (×), and (□) and for MIBC/2M NaCl solutions by us (◊) and Chi Phan (●). The 15 mM and 20 mM labels represent the topmost monolayer saturation concentrations in the presence and absence of 2 M NaCl, respectively. Panel (b): surface excess values calculated by Gibbs equation using third-order polynomial fitting for MIBC (●) and MIBC/2M NaCl (□) solutions.

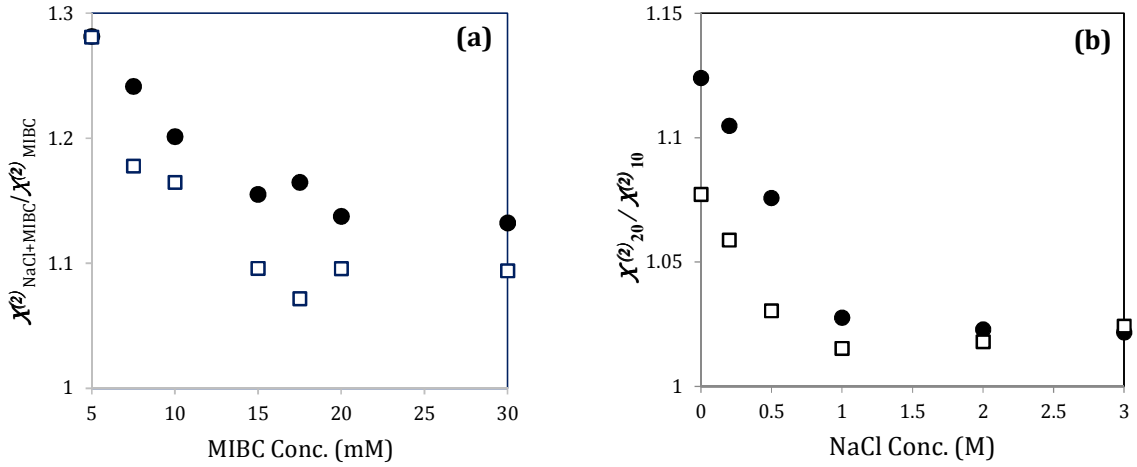

Figure 5. (a) Variation in the ratio between the susceptibility in the presence of 2 M NaCl ($\chi^{(2)}_{NaCl+MIBC}$) and that in the absence of salt ($\chi^{(2)}_{MIBC}$) with MIBC concentration, and (b) Variation in the ratio between the susceptibility in the presence of 20 mM MIBC ($\chi^{(2)}_{20}$) and that in the presence of 10 mM MIBC ($\chi^{(2)}_{10}$) with NaCl concentration under (●) ssp and (□) ppp polarization combinations.

Table 1. Peak features extracted from the spectral fitting results for a 30 mM MIBC solution.

Peak assignment	ω_q (cm^{-1})	ssp		ppp	
		A_q	Γ_q	A_q	Γ_q
CH_2 υ_s	2838	151.47	13.05	-	-
CH_3 υ_s	2875	556.57	7.93	30.50	4.76
CH_2 υ_{as}	2920	31.62	6.01	-	-
CH_3 υ_{as}	2966	115.44	6.83	405.82	7.37
CH_2 υ_{FR}	2906	-155.72	4.12	117.85	12.63
CH_3 υ_{FR}	2944	437.68	10.09	119.05	8.74

Table 2. The adsorption parameters extracted from surface tension plots using Gibbs isotherm

Ads. Parameter	MIBC	MIBC/NaCl
Γ_m ($\times 10^6$ mol/m^2)	4.4[a] 4.2[b]	5.1[c] 5.0[d]
A_{min} (Å^2/molecule)	37	32
pC_{20}	1.75	2.15
γ_s (mN/m)	51	47

[a] $\gamma = -24.94 \log C + 82.683$

[b] $\gamma = -0.8106 \times (\log C)^3 - 5.0804 \times (\log C)^2 - 6.5192 \times \log C + 69.482$

[c] $\gamma = -28.86 \log C + 80.817$

[d] $\gamma = -0.4728 \times (\log C)^3 - 6.654 \times (\log C)^2 - 10.992 \times \log C + 70.001$